*Supplemental methods*

*Cloning of ApoE constructs:*

Quickchange site directed mutagenesis introduced stop codons into the pET30(+) vector containing His-tagged monomeric ApoE (a gift from Jianjun Wang, described in [48]) at positions 170 and 239. ApoE3 1-191 was generated by PCR from the 1-238 template using the forward primer 5'-GGGAATTCCATATGCACCATCATCATCATCAT and reverse primer 5'-CCGCTCGAGTTACCGCACGCGGCCCTGTTCC and ligated into a pET23b vector with NdeI/XhoI restriction sites. Overlap extension PCR cloning was used to incorporate the BirA peptide and linker sequence (GLNDIFEAQKIEWHEGGSGGS) at the N-terminus of ApoE upon expression. Briefly, two initial PCR reactions created overlapping termini of linear insert containing BirA sequence at 5' end of APOE (N-terminal product) and a vector backbone. A second PCR reaction using the products from the initial PCR reactions created the final plasmid containing BirA-GGSGGS-ApoE4. Insert Primers: Sense - 5' CATTTTCGAG GCGCAAAAAA TTGAATGGCA TGAAGGAGGA AGCGGCGGTT CCAAGGTTGA ACAGGCTGTT GAAACTGAAC CGG 3', Antisense - 5' GCAAGCTTGT CGACGGAGCT CGAATTCAGT GATTGTCG 3' Vector Primers: Sense - 5' CGACAATCAC TGAATTCGAG CTCCGTCGAC AAGCTTGC 3', Antisense - 5' CCTCCTTCAT GCCATTCAAT TTTTTGCGCC TCGAAAATGT CATTCAGGCC GGGTCCTTGA AATAGCACTT CCAGGTCGTC G 3'. All constructs were sequence-verified.


**Methods for Computational Structure Analysis of TREM2 Ig and sTREM2**
**Structures for TREM2-Ig and sTREM2**
Of the structures available in the protein data bank for the TREM2 IG domain,(*1, 2*) we chose the highest resolution 2.2Å crystal structure expressed in HEK-293S cells (PDBID: 5ud7) as our starting model of the common variant human IG domain. The starting model was first energy minimized by steepest descent followed by conjugate gradient in AMBER14 (*3, 4*) to obtain an initial structure of the TREM2 Ig domain. From this model, we used the *automodel* class of the software package Modeller to introduce the missing amino acids (130-157) of the C-terminal stalk found in sTREM2 as a series of 50 random coils.(*5*) These procedurally generated

structures were then ranked by discrete optimized protein energy (DOPE) score,(*6*) and the top 5 were introduced to Modeller's built-in loop refinement to generate a new list of 50 refined models (10 from each initial structure). The refined models were again ranked by DOPE score and the new top 5 were minimized with 500 rounds of steepest descent and 500 of conjugate gradient. From there, each model was analyzed using the NIH Structural Analysis and VErification Server (SAVES) (http://nihserver.mbi.ucla.edu/SAVES), and the one with the most favorable packing quality and bond structure was selected as our model of sTREM2.

## MD Simulations

Molecular dynamics (MD) simulations for the TREM2 Ig domain with (sTREM2) and without the C-terminal stalk were performed with AMBER14 using the ff14SB force field.(*3, 4*) The MD simulations were performed in a periodic box with 2 nm of TIP3P water and 150 mM NaCl between the protein edge and the box boundary to reduce periodicity artifacts and approximate physiologic conditions. Additional $Cl^-$ or Na+ ions were added to each system at random positions to neutralize the protein charge. We first performed steepest descent minimization of the solvent water with the protein and ions restrained. This was followed by equilibration of the minimized water molecules with the protein and ions restrained at constant number-pressure-temperature at 50 K and 1 bar for 20 ps. The systems were heated via a series of 10 ps constant number-volume-temperature MD simulations at 50, 100, 150, 200, 250, and 300 K. MD production simulations of 100 ns at number-pressure-temperature of 300 K and 1 bar were performed for each simulation. SHAKE constraints with relative tolerance of $1 \times 10^{-5}$ were used on all hydrogen-heavy atom bonds to permit time steps of 2 fs. Electrostatic interactions were calculated by the particle-mesh Ewald method. The Lennard-Jones cutoffs were set at 1.0 nm.

## MD Analysis

To determine the degree of equilibration in our simulated systems, RMSD was calculated over the trajectory of each simulation and frames clustered with the *dbscan* algorithm(*7*) to determine the initial simulation time needed for each simulation to reach system equilibration. The *dbscan* algorithm also generates an average structure for the population of the equilibrated cluster called a centroid, which can be overlaid to show changes in conformation between the simulated models. Based on RMSD analysis, the first 15ns of each simulation were discarded as equilibration time and the last 85ns reserved for further analysis. To characterize the effects of the C-terminal tethering stalk on secondary structure of the TREM2 Ig domain based on the equilibrated MD simulation trajectories, we examined changes in secondary structure using the DSSP method to assign the most likely class of secondary structure for each residue in the protein at each frame.(*8*) These calculations are presented as a percent of time that each residue spends occupying a particular secondary structure. To characterize the differences in conformational flexibility caused by presence of the tethering stalk on the TREM2 Ig domain, we calculated root mean squared fluctuations (RMSF) of individual alpha carbons for each residue along the TREM2 backbone over the equilibrated portion of each simulation trajectory. To determine which components of movement contribute most to the total motion at equilibrium, we separated the equilibrated motions into principal components using essential dynamics.(*9, 10*) Results of this analysis are shown as porcupine plots showing each residue's contribution to the overall motion in the first principal component. To analyze the degree of correlated motions between residues for TREM2-Ig with and without the tethering stalk over

the equilibrated MD simulation trajectories, we generated a dynamic cross correlation map (DCCM) for TREM2-Ig with and without the tethering stalk. Each point in the DCCM represents correlation between a pair of residues and can have a value ranging from −1 to 1, where −1 represents perfectly anticorrelated motion, 1 represents perfectly correlated motion, and 0 represents perfectly independent motion.

## Results

To determine whether presence of the C-terminal stalk found in sTREM2 (residues 130-157) was likely to affect the structure or dynamics of the TREM2 Ig domain, we ran short MD simulations of the Ig domain with and without this stalk. The missing residues of the stalk were generated as a random coil on the C-terminus of the TREM2-Ig crystal structure (PDBID: 5UD7) using Modeller software. Based on RMSD profiles and clustering analysis of 100 ns simulation trajectories, both models of TREM2 equilibrated within 15 ns, leaving 85 ns for analysis (**Fig S6A**). Based on the equilibrated portion of the two models, the secondary structure of the TREM2 Ig domain is not significantly affected by addition of the unstructured stalk region, with only a small decrease in preference for the 3-10 turn visible in the βE-βF loop (**Fig S6B**). On the other hand, addition of the tethering stalk increases conformational flexibility across the entire TREM2 Ig domain, which can be seen by an increase in RMSF and an increase in the magnitude of both correlated and anti-correlated motions across the entire Ig domain (**Fig S6C, E**). This increased flexibility also presents as spreading of the first principal component of motion across the Ig domain, rather than just the lateral loops, following introduction of the stalk (**Fig S6D**). However, despite the increase in total motion across the Ig domain caused by addition of the tethering stalk, inter-residue distance maps and overlays of the centroid conformations show slight changes in overall conformation of the TREM2 Ig domain (**Fig S6F, G**). Altogether, these data suggest that while the presence of the C-terminal tethering stalk in sTREM2 seems to increase the total motion of the Ig domain, it does not seem to affect its overall structure or conformation.

1.    D. L. Kober *et al.*, Neurodegenerative disease mutations in TREM2 reveal a functional surface and distinct loss-of-function mechanisms. *Elife* **5**, e20391 (2016).
2.    A. Sudom *et al.*, Molecular basis for the loss-of-function effects of the Alzheimer's disease-associated R47H variant of the immune receptor TREM2. *J Biol Chem* **293**, 12634–12646 (2018).
3.    D. A. Case *et al.* (University of California, San Francisco, 2015).
4.    J. A. Maier *et al.*, ff14SB: Improving the Accuracy of Protein Side Chain and Backbone Parameters from ff99SB. *J Chem Theory Comput* **11**, 3696–3713 (2015).
5.    A. Fiser, R. K. Do, A. Sali, Modeling of loops in protein structures. *Protein Sci* **9**, 1753-1773 (2000).
6.    M. Y. Shen, A. Sali, Statistical potential for assessment and prediction of protein structures. *Protein Sci* **15**, 2507-2524 (2006).
7.    M. Ester, H.-P. Kriegel, J. Sander, X. Xu, paper presented at the Proceedings of 2nd International Conference on Knowledge Discovery and Data Mining, 1996.
8.    W. Kabsch, C. Sander, Dictionary of protein secondary structure: pattern recognition of hydrogen-bonded and geometrical features. *Biopolymers* **22**, 2577–2637 (1983).

9.    C. C. David, D. J. Jacobs, Principal component analysis: a method for determining the essential dynamics of proteins. *Methods Mol Biol* **1084**, 193–226 (2014).

10.    A. Amadei, A. B. M. Linssen, H. J. C. Berendsen, Essential dynamics of proteins. *Proteins: Structure, Function, and Bioinformatics* **17**, 412–425 (1993).
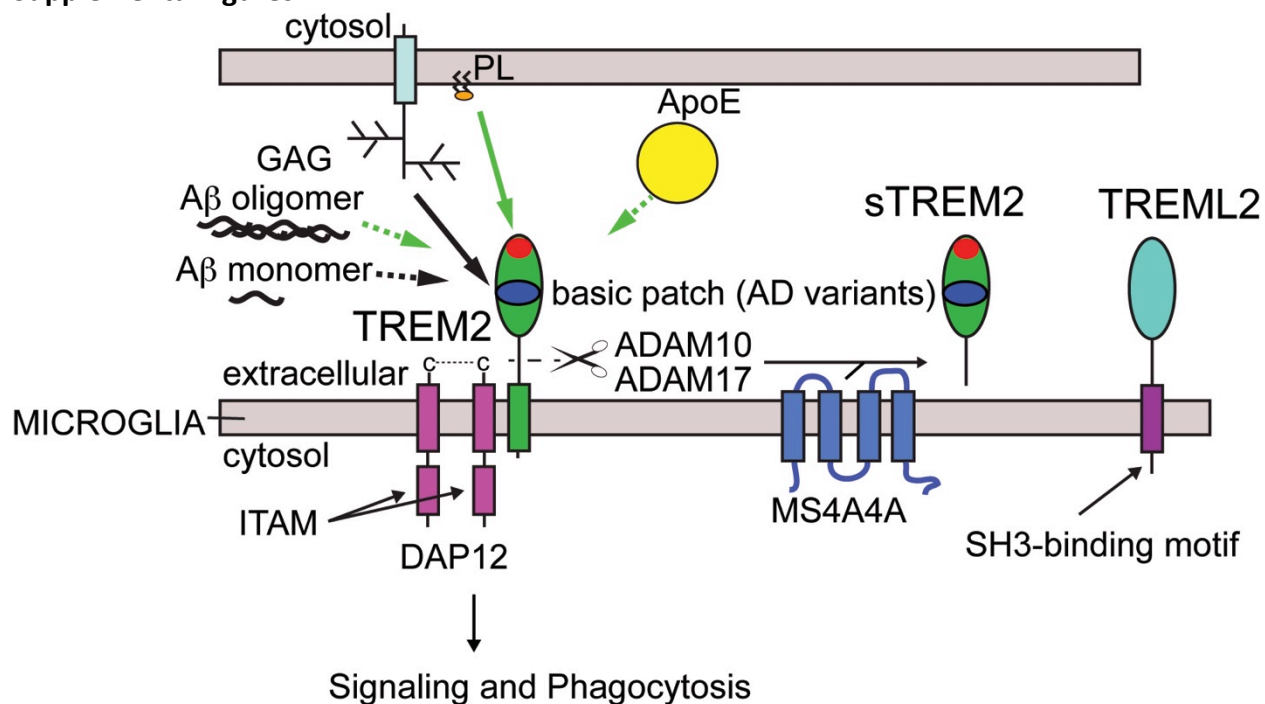
**Figure S1.** Graphic summary of known binding partners for TREM2 with proven or potential relevance to AD previous to this paper. Interaction surfaces mapped by either crystallography or mutation and binding studies are shown as solid lines whereas direct interactions that have been shown but not mapped are shown as dashed lines. Green lines indicate interactions that result in TREM2 signaling through DAP12. Black lines indicate direct interactions that have not yet been shown to induce signaling. Phospholipids engage the hydrophobic patch. Glycosaminoglycans (GAGs) engage the basic patch. Soluble TREM2 (sTREM2) can be produced by proteolytic cleavage by ADAM10 and ADAM17 or by alternate transcripts. sTREM2 levels appear to be modulated by MS4A4A. TREM-like-2 (TREML2) is a single pass transmembrane protein expressed on microglia with an ectodomain consisting of an Ig fold and stalk similar to TREM2.
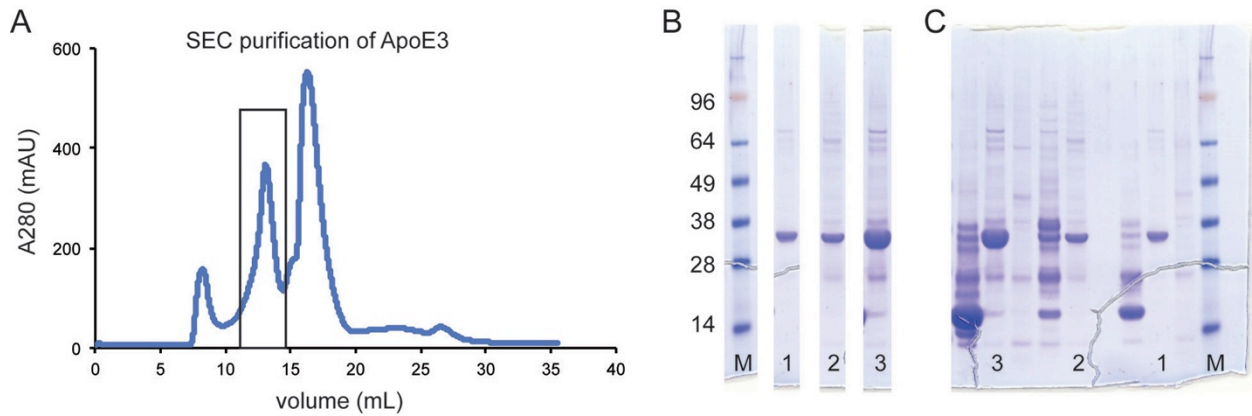
**Figure S2. SEC purification and SDS-PAGE of non-lipidated ApoE proteins. A)** ApoE3 purification by size-exclusion chromatography (SEC) using a superdex s200 column. Chromatograms for ApoE2 and ApoE4 were nearly identical. Black box denotes peak for ApoE3. **B)** SDS-PAGE analysis of purified: 1- ApoE2; 2- ApoE3; 3- ApoE4. All samples were run on the same gel but non-related lanes were cropped out and the remaining lanes vertically aligned for clarity. **C)** The complete intact gel that was cropped for B). Lanes used in B) are labeled identically.

## ApoE3 Lipidation
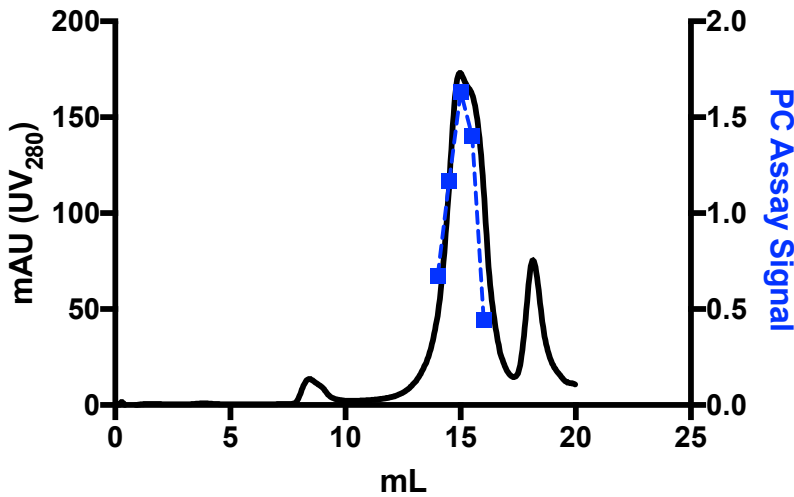


**Figure S3. SEC purification and analysis of lipidated ApoE3.** ApoE3 complexed with DPPC particles was purified by SEC (Superose 6) before BLI assays. The major peak was collected, and a PC assay signal (blue markers) from the collected fractions correlated with the UV peak, showing the presence of PC in the ApoE lipoparticles. Buffer alone and non-lipidated ApoE3 had no signal (not shown).
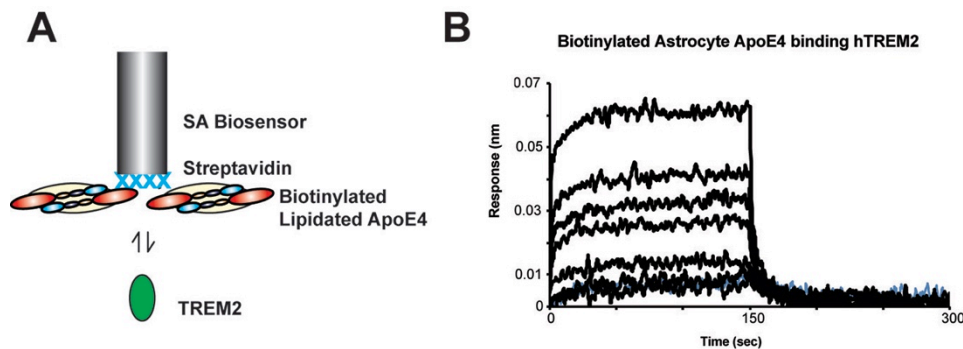


**Figure S4. Biotinylated astrocyte derived ApoE4 binding to TREM2 using BLI.** Lipid-loaded ApoE4 affinity purified from astrocytes was biotinylated using EZ-link PEG4 biotin and immobilized on a streptavidin biosensor. Purified TREM2 was in the wells at a concentration range of 3-200 μM. Sensorgrams were subtracted by double referencing. Lipid composition of ApoE lipoparticles did not appear to dramatically enhance binding to TREM2, as astrocyte-derived ApoE4 lipoparticles bound similarly to ApoE4:DPPC particles. However, the analysis was not exhaustive and may have been influenced by the orientation of the experiment.
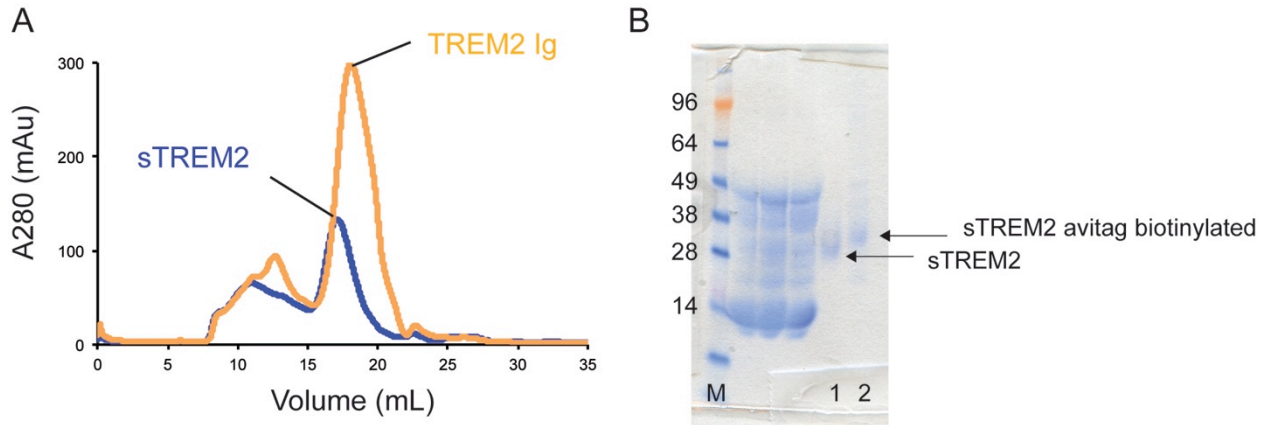
**Figure S5. Purification and SDS-PAGE analysis of sTREM2 proteins used in binding experiments. A)** Size exclusion chromatogram (Superdex200 10/300GL) for sTREM2 and TREM2 Ig. sTREM2 appears to elute as a monomer, similar to TREM2 Ig. **B)** SDS-PAGE analysis of purified proteins. Lanes labeled as follows: M = molecular weight markers (kDa); 1 = sTREM2; 2 = avitag sTREM2 after site-specific biotinylation.
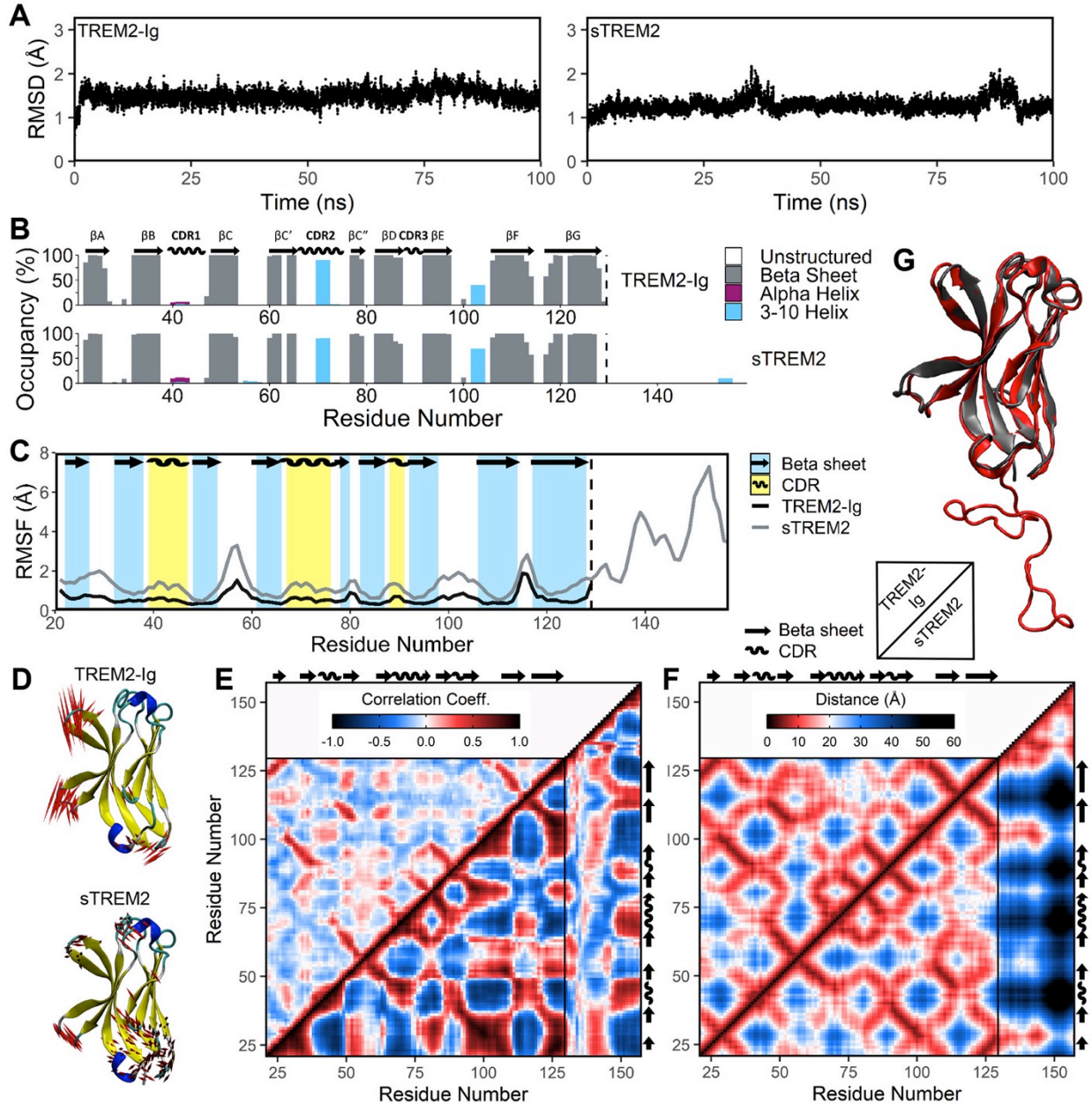
**Figure S6. Molecular dynamics (MD) simulations of the TREM2 immunoglobulin domain with (sTREM2) or without (TREM2-Ig) the membrane-tethering stalk (residues 130–157) identify small differences in flexibility but not secondary structure or conformation. (A)** Simulations equilibrate within 15 ns based on RMSD profiles for the TREM2 Ig domain with and without its stalk region. The starting conformation for the sTREM2 model was generated using Modeller software by adding the missing residues of the tethering stalk as a random coil to the C-terminus of the TREM2-Ig crystal structure (PDBID: 5UD7). **(B)** The preferences of residues in the TREM2 Ig domain for three major classes of secondary structure are not significantly affected by addition of the unstructured stalk region. Percent occupancy in a secondary structure for each residue was assigned as percent of time that residue spends as β-sheet (gray), α-helix (pink), or 3-10 helix (cyan) across the equilibrated portion (15–100 ns) of the MD

trajectory. **(C)** Addition of the tethering stalk increases conformational flexibility across the entire TREM2 immunoglobulin domain. Root mean squared fluctuation (RMSF) is a measure of motion of each residue individually averaged over the equilibrated portion of the trajectory. The panel shows an overlay of TREM2-Ig (black lines) and sTREM2 (gray line) for comparison with reference β-strands (blue; arrows) and CDRs (yellow; waves) highlighted. **(D)** Porcupine plots showing the first principal component of motion for residues in the TREM2 Ig domain with and without effects of the tethering stalk. The increased flexibility over the Ig domain seen by RMSF causes contributions to the first principal component to spread across the TREM2 Ig domain. **(E)** Dynamic cross-correlation maps (DCCMs) for TREM2 with and without the tethering stalk. The increased flexibility over the Ig domain seen by RMSF translate to increased magnitude of both correlated and anti-correlated motions across the TREM2 Ig domain. In the DCCMs, 1 represents perfectly correlated motion (darkest red) and −1 represents perfectly anti-correlated motion (darkest blue). **(F)** Inter-residue distance maps show that the increase in motion seen by RMSF, PCA, and DCCM does not cause any noticeable changes in the average distances between residues. In the distance maps, nearby residues are shown in red and more distant residues in blue. **(G)** Aligning the centroid representations of the TREM2-Ig domain with (red) and without (gray) the tethering stalk shows that its addition does not cause any significant conformational change.
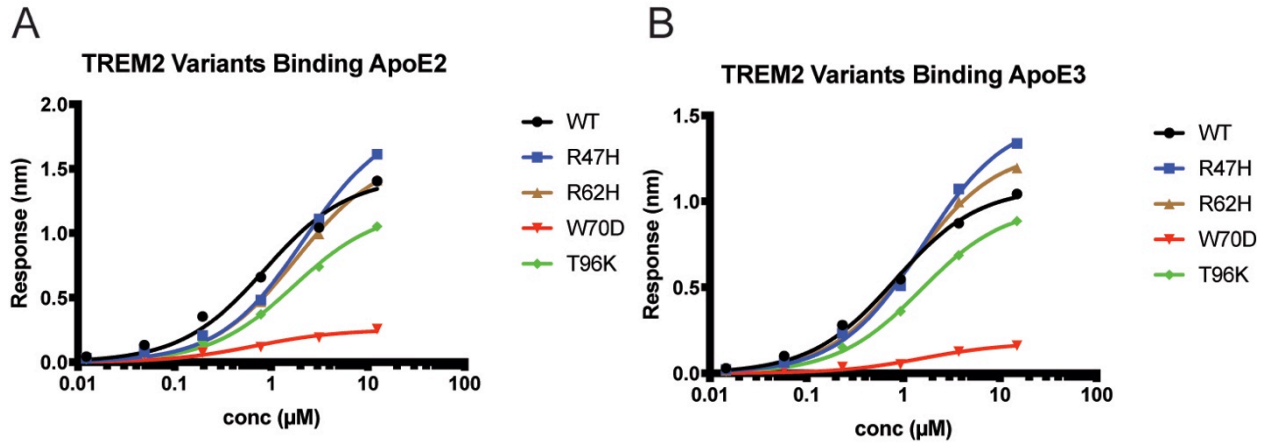
**Figure S7.** Steady-state binding of **A)** ApoE2 and **B)** ApoE3 to WT and TREM2 variants immobilized on SA BLI biosensors.

**hTREM2 W70D preparative SEC**
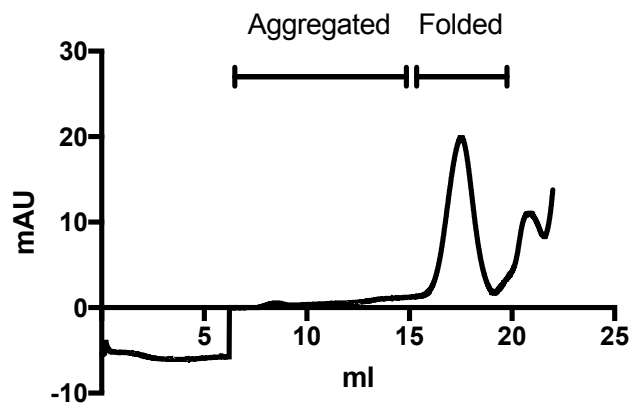
**Figure S8. W70D mutations does not cause aggregation as assessed by SEC.** W70D preparative SEC trace. The variant elutes in the fractions corresponding to folded TREM2, with minimal aggregated protein.
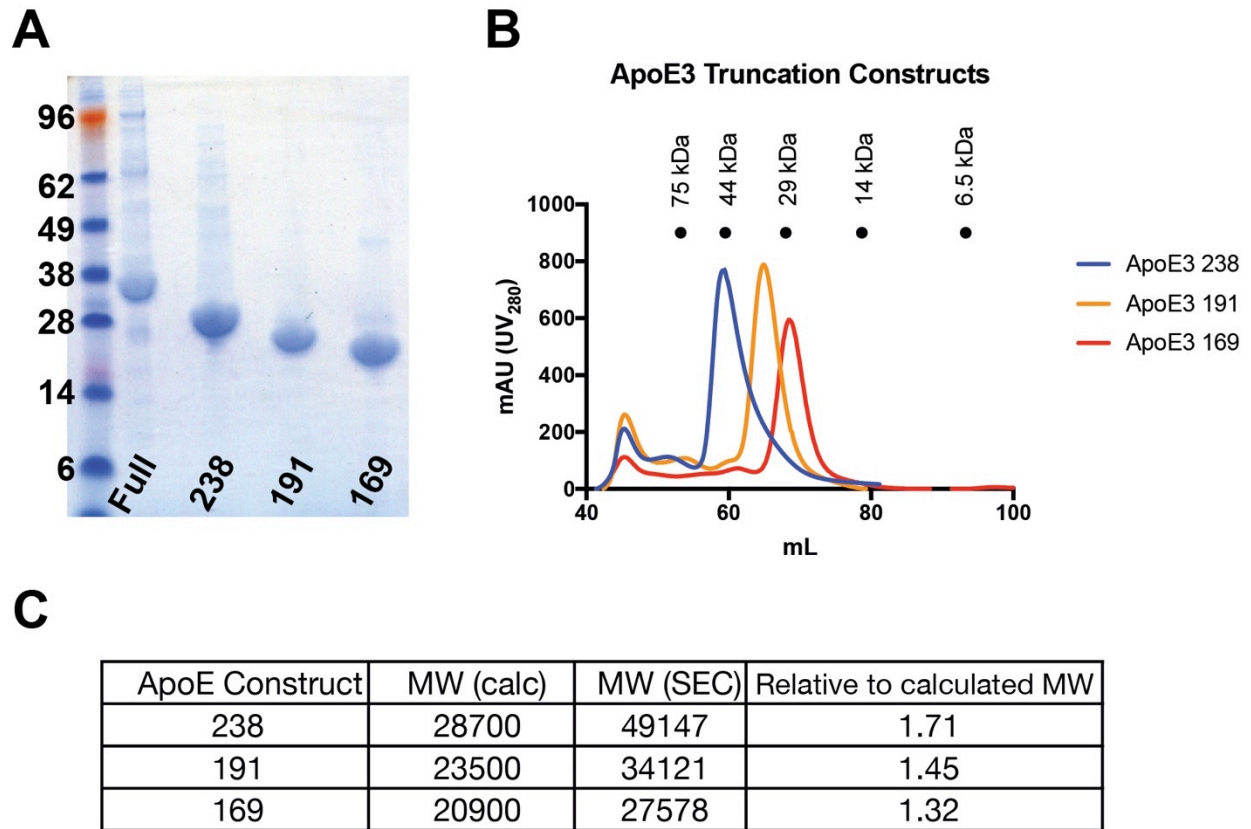
**Figure S9. Purification and behavior of ApoE3 truncations. A)** Purity of full-length ApoE3 truncations used in Figure 3 is shown by SDS PAGE. **B)** SEC traces of ApoE3 truncations and elution volumes of molecular standards. **C)** Table of calculated and experimental (SEC) MW of ApoE truncations. All truncations run about 1.5x their expected size, below a dimer size. The apparent increase is likely due to their elongated, non-globular structure.
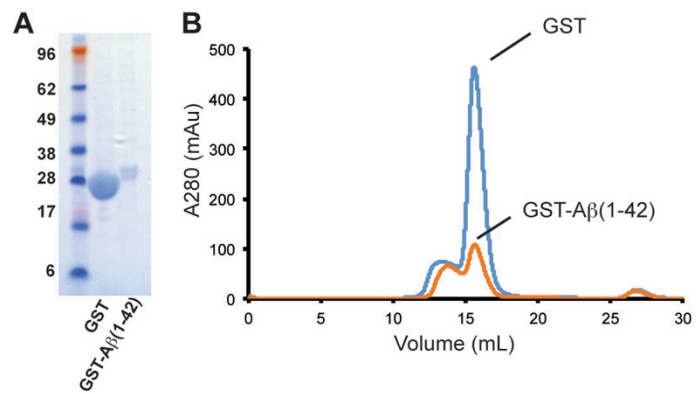
**Figure S10. A)** SDS-PAGE gel of GST and GST-A$\beta_{42}$ used in the experiment shown in Figure 5C,D. Molecular weight markers are labeled in kDa. **B)** Size exclusion chromatography chromatograms for GST and GST-A$\beta_{42}$ used in experiments in Figure 5C,D.

Supplementary Table 1

| Region (Residues) | | CDR Forward | | | CDR Reverse | | |
|---|---|---|---|---|---|---|---|
| TREM2 | ApoE | Match | Start | End | Match | Start | End |
| CDR1 (39-46) | LDLR Region (130–149) | 75.00% | 134 | 141 | 62.50% | 134 | 141 |
| | Hinge Region (192–238) | 62.50% | 192 | 199 | 75.00% | 192 | 199 |
| CDR2 (69-76) | LDLR Region (130–149) | 87.50% | 134 | 141 | 87.50% | 135 | 142 |
| | | 87.50% | 137 | 144 | 100.00% | 138 | 145 |
| | | 87.50% | 140 | 147 | 75.00% | 141 | 148 |
| | Hinge Region (192–238) | | | | 75.00% | 192 | 199 |
| | | | | | 62.50% | 193 | 200 |
| | | 75.00% | 194 | 201 | 75.00% | 195 | 202 |
| | | 62.50% | 199 | 206 | 62.50% | 199 | 206 |
| | | 62.50% | 200 | 207 | 62.50% | 200 | 207 |
| | | | | | 62.50% | 201 | 208 |
| | | 75.00% | 202 | 209 | 75.00% | 203 | 210 |
| | | | | | 62.50% | 204 | 211 |
| | | 62.50% | 206 | 213 | 62.50% | 206 | 213 |
| | | 62.50% | 208 | 215 | 62.50% | 208 | 215 |
| | | 62.50% | 210 | 217 | 62.50% | 210 | 217 |
| | | | | | 75.00% | 215 | 222 |
| | | 87.50% | 217 | 224 | 87.50% | 218 | 225 |
| | | 75.00% | 220 | 227 | 75.00% | 221 | 228 |
| | | 75.00% | 222 | 229 | 75.00% | 223 | 230 |
| | | 87.50% | 225 | 232 | 87.50% | 226 | 233 |
| | | | | | 75.00% | 229 | 236 |

Rows with colored text represent top the predicted binding site(s) between a pair of regions. Colors match those used in Figure 2.

**Table S1.** Binding sites on the LDLR-binding region and hinge region of ApoE predicted by hydropathy mapping to be >60% complementary to forward or reverse peptides of the TREM2 hydrophobic surface.